

Experimental analysis of additively manufactured foamed polylactic acid structures under compression loading

Armin Yousefi Kanani^{a*}, Andrew Kennedy^a

^a Department of Engineering, Engineering Building, Lancaster University, Lancaster, LA1 4YW, UK

* Corresponding author (email address: a.yousefikanani@lancaster.ac.uk)

Abstract

This work evaluates the potential for foamable polymer filaments to be used to make lightweight, energy-absorbing structures using additive manufacturing. In order to achieve this, a commercial, foamable polylactic acid filament was extruded using material extrusion (MEX) process to make parts for compression testing. It was found that a maximum foam expansion could be achieved at an extrusion nozzle temperature of 220°C, but that to achieve dimensional accuracy, the material flow rate through the nozzle had to be adjusted by decreasing the extrusion multiplier value. In a novel approach, accurate and faster builds could be achieved by decreasing the infill instead.

When compared with porous structures achieved by using partial infilling instead or as well as foaming, all materials were found to follow the same power-law function of the solid fraction. These trends indicated that the mechanical response was, within experimental scatter, a function of the overall solid fraction and not influenced by whether the porosity was within or between **the raster lines**. Although there was no apparent benefit to the mechanical performance in introducing porosity into a polymer via foaming, foamable filaments are desirable if stiff, lightweight structures with low fractions of interconnected porosity are required and can be used in combination with infilling to produce low-density structures that would be highly suitable for cores in novel lightweight sandwich structures.

Keywords: additive manufacturing; Material extrusion; foamable polylactic acid filament; porous structures; lightweight structures

1. Introduction

Foam materials, which are made up of both a solid and a gas phase [1], are found in various natural and man-made items, owing to their cellular structure, providing a wide range of beneficial properties [2]. Foam properties are linked to their inherent properties, density, and foam structure [3]. They offer numerous benefits over denser polymer materials, including low density, good heat insulation, effective sound insulation, good energy absorption and high specific strength and stiffness [3]. These properties are extremely useful in many industrial applications, which include aerospace or automotive parts, sporting equipment and thermal insulation [4][5].

The fundamental process of producing a polymer foam usually begins with two materials, the blowing agent and the polymer itself. Blowing agents are classified into two separate groups, physical blowing agents (PBA) and chemical blowing agents (CBA) [1][3]. PBAs are liquids/gases that dissolve directly into the polymer matrix, whereas CBAs are typically solids that dissolve or distribute before releasing gas via thermal decomposition [1]. Carbon dioxide is the most commonly employed fluid (both as a PBA in its own right and as the gas emitted by many CBAs). When it is used as a PBA, there are two major processes in the foaming process. First sorption, the dissolution of carbon dioxide in the polymer matrix under pressure to form a polymer/gas solution, followed by bubble nucleation and growth when the pressure is reduced. [6]. The same basic process is performed when making a foam using a CBA, but the bubble nucleation begins when the CBA and polymer mixture is heated. When the CBA decomposes at high temperatures, gases are trapped inside the structure, causing bubble nucleation [7]. While a large range of possible CBA's are being sold commercially, many contain different ratios of the same base chemicals. The most common chemicals used to create these blowing agents are citric acid, sodium bicarbonate and azodicarbonamide (ADC) [8].

The production of the polymer foams is well established using injection or compression moulding methods. However, these technologies require tooling to fabricate complicated parts, which may be costly and time-consuming [9]. Therefore, new production technologies may be necessary for the future, owing to the requirement to employ new raw materials to produce complex geometries. Research on additive manufacturing (AM) shows that material extrusion (MEX) process is one of the most commonly used methods for creating complicated functional parts in polymers that are too complex for traditional manufacturing processes [10]. MEX 3D printers function by extruding thermoplastic filaments like ABS (Acrylonitrile Butadiene Styrene) and PLA (Polylactic Acid) through a heated nozzle in a layer-by-layer manner on the build platform until the part is complete. This approach has advantages, including low-cost equipment and raw materials, easy post-processing and functionalisation using composites, and the ability to combine polymers. However, MEX process has certain drawbacks, such as poor print quality compared to the other additive manufacturing methods and is a slow process when large numbers of parts are required.

In recent years the interest in using MEX 3D printers to produce low-density porous polymeric structures has grown significantly. Gases, such as CO₂ or nitrogen, have been used to generate porous polymeric materials [11]. Zhou et al. [12] used a partial gas saturation technique to fabricate a functionally graded porous polymer by controlling the concentration profile inside the polymer. Song et al. [13] used a combination of fused deposition modelling (FDM) and gas foaming technology to fabricate hierarchical scaffolds with tailored macro/micro-porosity architectures for bone tissue applications. In this method, the combination of Polyvinyl alcohol (PVA) and PLA were used to create macropores then scaffolds were subjected to gas foaming to create micropores. Choi et al. [14] utilised the combination of CBA, a chain extender (CE) and Polylactic acid (PLA) to produce foamable filament to fabricate scaffold for medical application using FDM 3D printers. The CE reaction was used to enhance the foam stability of PLA, rheological properties, mechanical properties, and molecular weight by using an optimum amount of CE (here 1.5 wt%). In addition, the CBA was used in the mixture in order to introduce a pore structure. Damanpack et al. [15] studied the printing of commercial Colorfabb foamed PLA filament and found that the size and quantity of the gas bubbles increased when the deposition temperature was increased in the range of 215 °C to 250 °C. At the maximum foaming temperature (250 °C), the flow rate was reduced to 35% of normal to compensate for foam expansion. Other investigators [16] [17] have tested the same material and have observed differing optimum flow rates and temperatures using different MEX printing systems.

This study aims to understand the effect of the deposition temperature on the compressive properties of a commercial foamable PLA filament printed using the material extrusion process. It also aims to compare the performance of these novel materials with foamed and non-foamed structures by introducing void between raster line using different infill percentages. Focus is mainly directed to the potential for these materials to be used as lightweight and energy-absorbing structures.

Experimental Methods

Commercial foamable PLA filament (LW-PLA, Colorfabb) with a diameter of 1.75 mm was used. This filament contains an unknown fraction of the foaming agent, which is activated above a critical temperature. PLA samples were printed using a Flashforge Finder 3D printer with a nozzle diameter of 0.4 mm. The geometries of the 3D printed samples were modelled using Solidworks software, and Simplify3D software was used to generate the G-code for the 3D printer.

In order to focus on the influence of the print temperature on foaming expansion, build parameters such as layer height, print speed, travel speed, number of tops and bottom layers and perimeter shells, fill pattern and raster angle were kept constant. To control the amount of material deposited, the extrusion multiplier (EM) and degree of infill (DI) were varied. The extrusion multiplier is a fractional scaling of the material flow rate through the nozzle, and the infill percentage is a measure of the amount of material

that fills the interior of the build. Table 1 summarises the fixed and variable factors used in the experiments.

Table 1: Fixed and variable print parameters

Fixed Factors		Variable Factors	
Nozzle diameter (mm)	0.4	Temperature (°C)	200, 210, 220, 230 and 240
Printing Speed (mm/s)	50	Extrusion Multiplier	0.9, 0.65, 0.5, 0.55 and 0.65
Travel speed (mm/s)	80		
Layer height (mm)	0.2		
Top and bottom solid layers	2	Infill Percentage (%)	100, 80, 50 and 20
Outline/perimeter shells	2		
Fill pattern	Rectilinear		
Raster angle	45/-45		

Hollow structures $20 \times 20 \times 10$ mm, with a wall thickness of 0.4 mm, were printed in order to find the optimum EM value at each printing temperature. The EM value was reduced, from 1.0, in increments of 0.05 until the thickness of the wall, measured using digital Vernier callipers, was within ± 0.05 mm of the 0.40 mm target. Solid cubes, $12 \times 12 \times 12$ mm, were also printed to confirm the dimensional accuracy for builds with the optimum EM. The density of these builds was also determined by dividing an object's mass by its volume (Figure 4). For each condition, three samples were built and measured and averages were taken.

Samples with dimensions 16mm x 16mm x 24mm were printed for subsequent compression testing, according to ASTM D695. The orthogonal orientation notation specified in ASTM 52921 was used to specify the sample orientations relative to the build plate. Samples were fabricated in the YX and ZX directions. The target sample dimensions and the build orientations are shown in Figure 1. Three different infill percentages (20%, 50% and 80%) were also used at two different deposition temperatures that were found during these trials to result in no-foaming (200 °C) and foaming (220 °C).

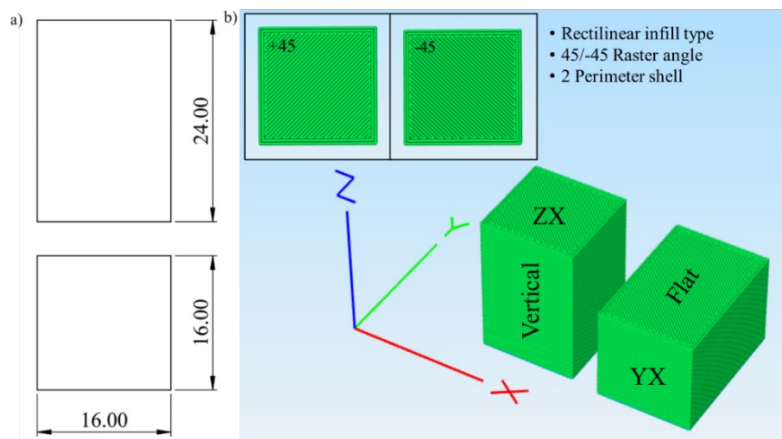


Figure 1: Sample geometry (a) and build configuration (b) for compressive testing (the XYZ coordinate system gives the global orientation of printing bed - are in mm)

Compression tests were performed using a universal electro-mechanical testing machine with a 100 kN load cell. Compression was performed along the long axis of the samples, at a speed of 2.4 mm/min, resulting in compression perpendicular (\perp) to the build layers for samples labelled as ZX and parallel (\parallel) to the build layers for samples labelled YX. A non-contact optical method (Imetrum system) was used, which tracks the movement of patterns on the sample to calculate displacement and strain. Stress-strain data were used to calculate the Young's Modulus and compressive yield strength. The yield point was defined as the 0.05% proof stress, and Young's modulus was calculated from the gradient of the linear portion of the stress-strain between 25 and 75% of the yield point. The energy absorbed (in J/m^3) up to 30% strain was determined from the area under the curve to this point. The energy absorption efficiency was calculated as the ratio of this energy to the product of the strain and either the stress at 30% strain or the yield stress, whichever was larger.

Results and discussion

Figure 2 shows microscope images of the difference between **single raster line** printed at 200°C and 220°C. Since the as-received filament is smooth, and small blister-type structures are seen on **the raster line** printed at 200°C, there is evidence of a small amount of foaming even at this temperature. It should be noted that adequate printing could not be performed on the printer used in this study at temperatures below this owing to poor adhesion to the bed. For printing at 220°C, the blisters become near spherical bubbles and widespread, as also observed in [19], leading to a highly roughened surface.

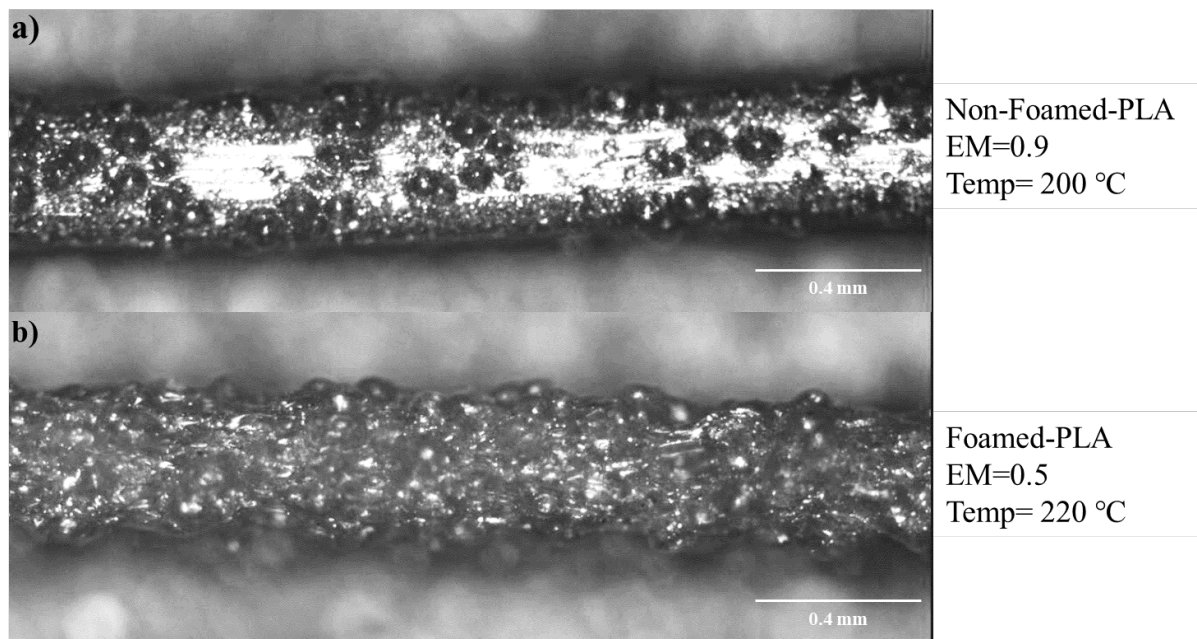


Figure 2: Microscope images of 3D printed samples with two different deposition temperatures (a) 200 °C and (b) 220 °C

Figure 3 shows the influence of the EM on the wall thickness. Printing at 200°C, below the expected temperature for foaming, and with an EM=0.9, yields an accurate part. Reducing the EM decreases the

track width (wall thickness) below the set value of 0.4 mm. An EM value less than one might suggest a small degree of expansion of the molten foamable PLA at this temperature. To account for the much larger foam expansion when printing at 220°C requires a decrease in the EM to 0.5.

Foaming is expected to occur as the filament melts in the cavity behind the nozzle opening, within the extrusion head. If the flow rate of filament to this cavity is too high (the EM is too high) for the foaming expansion to be accommodated, excess material will be ejected at the nozzle. Thus for the targeted track width, layer height and head speed, the actual track geometry will be oversized. The converse is also true for an EM that is too low. As the material is pre-foamed in the nozzle cavity, if the EM decrease balances the foaming expansion, such that the volumetric material flow rate is the same, the deposited track geometry should be as specified. This is broadly demonstrated by the tracks in Figure 2 of similar geometry, where a reduction in EM has compensated for foaming expansion.

Figure 3 shows the effect of the EM on the dimensions of solid cubes. At the correct EM, for a given speed and layer height, an MEX build of this type is typically accurate to ± 0.1 mm. This level of accuracy was achievable for the non-foamed cubes printed at 200°C with an EM = 0.9. A density of 1.24 g/cc at 200 °C (solid PLA is reported to be 1.3 g/cc in Ref [17]) does suggest some additional porosity between the deposited layers in the 3D build [18]. As in the case of the walled structure, if the EM is too high, the part will be "over-built", too low, and it will be "under-built". The optimum EM for the foamable filament (defined as when dimension accuracy was less than ± 0.5 mm from the target, as good as could be achieved for foamable filaments) is different at different build temperatures, 0.5 at 220°C, 0.6 at 240°C, indicating different degrees of foam expansion. Figure 4 shows the optimum EM and density at each temperature, where it is clear that minimum density, or maximum expansion, occurs at 220°C. Foam expansion, to a density of 0.59 cc, corresponds to a maximum observed increase in the volume of 110%, lower than the 150% reported in [17].

The degree of foam expansion will depend upon the melt temperature and the time it remains foamable. A balance must be struck to achieve optimum foam expansion through an adequate opportunity for foaming agent decomposition and pore nucleation and growth (curtailed by too low a melt temperature and too short a residence time) and preventing gas diffusion from the melt (which occurs if the melt temperature is too high [19] and the residence time too long). Although unaddressed in this study, process parameters such as bed temperature, nozzle size, layer height, and print speed can offer an additional means to optimise the foaming behaviour (and are likely to account for varying foaming performance on different machines). Maximising the expansion for this filament requires a comprehensive study of all the build parameters and possibly even the machine type, something that is beyond the scope of this study.

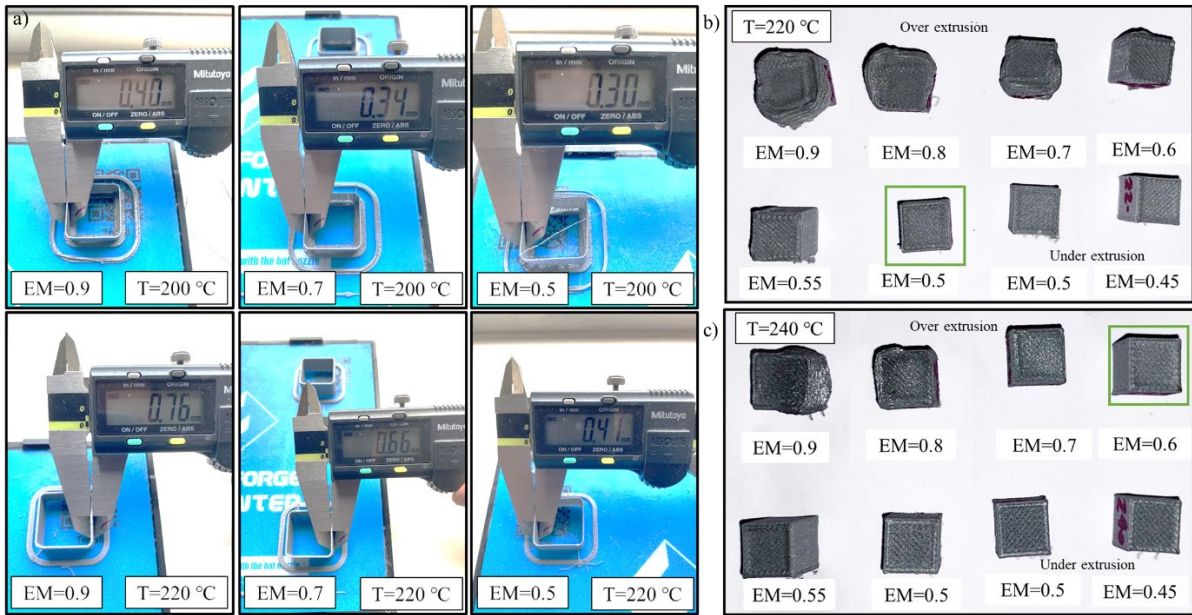


Figure 3: (a) Measurement of the wall thickness for hollow cubes. (b)-(c) solid cubes printed with different EM values for two representative deposition temperatures – optimum ER is boxed in green.

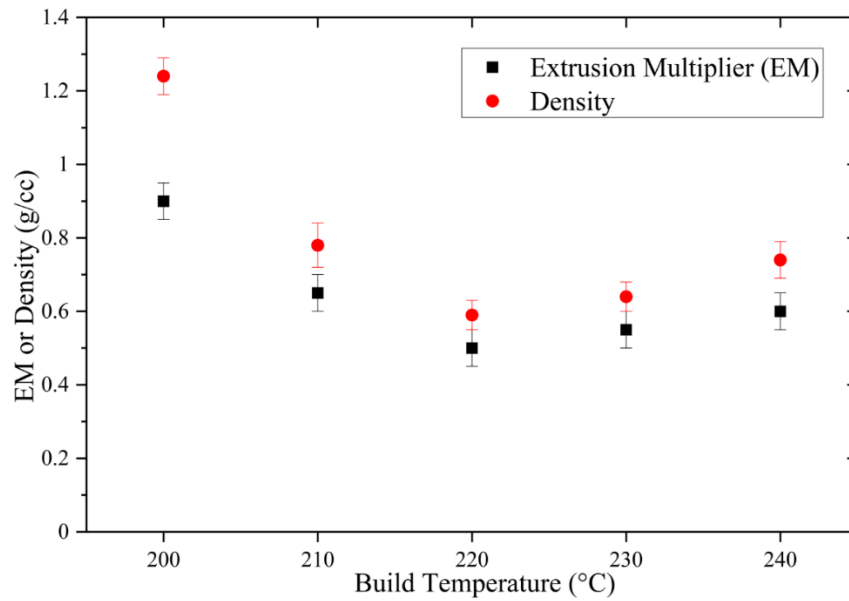


Figure 4: Optimum Extrusion Multiplier (EM) and density for five different build temperatures

Figure 5 presents representative stress-strain curves for samples made at each of the different build temperatures in the two test directions. Both materials show deformation that is broadly distinguished by three regions.

Both exhibit a linear-elastic region leading to initial maximum yield stress, followed by a prolonged plateau-like stage where crushing (or elasto-plastic behaviour in the case of the non-foamed material) takes place at relatively constant stress before a marked increase in stress at higher strains. The stress-strain curves for the non-foamed PLA, printed at 200°C, are typical of those observed in other studies [24-26], where the yield strength for 3D printed structures, with similar build parameters, lies between

50 - 60 MPa. Changing compression direction from parallel to perpendicular to the layers has little effect on the compressive yield strength.

It is clear that there is a big difference in the yield and plateau stresses for foamed and non-foamed samples. The yield stress is much higher (60 MPa) for the non-foamed PLA compared with the foamed material (< 30 MPa). There is a less clear trend in the yield strength as a function of density, but this may be clouded by the influence of build temperature on yield strength [20][21]. Changing the compression direction from parallel to perpendicular to the layers significantly decreases the yield stress for the foamed samples (which is clearer in Table 2), and it is also evident that for foamed samples compressed perpendicular to the layers (ZX), there is no load drop after yielding and the stress continually rises with strain. The rising nature of the stress-strain curves for foamed samples tested perpendicular to the layers means that they are less efficient energy absorbers. The non-foamed sample shows less anisotropy, but the large drop in stress after yielding results in a poorer energy absorption efficiency compared to foamed materials compressed parallel to the layers.

This different behaviour can also be observed in Figure 6. When the strain increases, foamed samples printed at the ZX direction crush without significant lateral volume expansion. This suggests that the voids in the raster lines are crushed, resulting in the densification of these ZX samples [22][23]. On the other hand, samples printed in the YX direction bulge at the centre when compressed, as do all non-foamed samples.

The foam samples are more sensitive to the print direction due to weaker bonding between raster lines caused by the uneven surface of the tracks (shown in Figure 2). Therefore, their performance depends on the direction of the raster lines (width or height) in relation to the applied force and the quality of the bonding area between the raster lines [24]. As shown in Figure 7, the better performance of the YX samples can be justified by the fact that the raster width (the longer length of the raster) is parallel to the applied force. The larger contact area in the width direction provides better adhesion between raster lines which helps them to absorb more energy and withstand higher force before yielding.

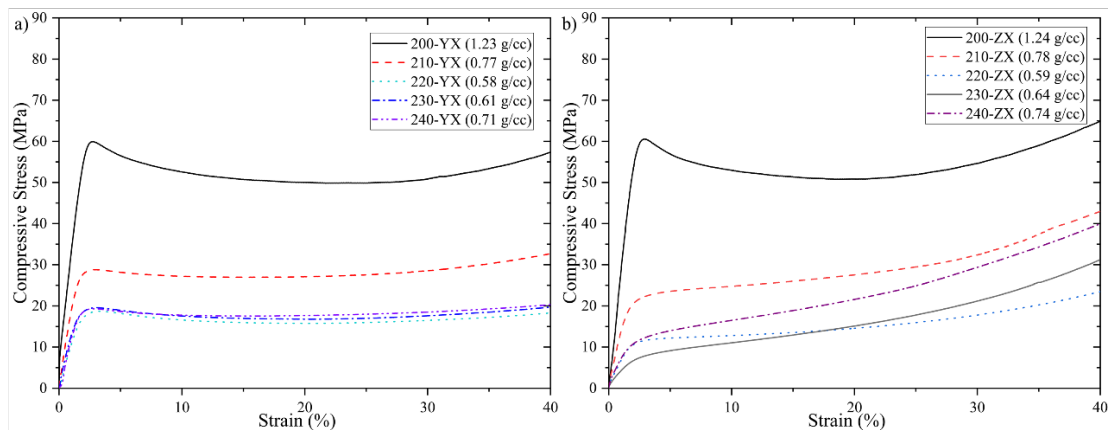


Figure 5: Stress-strain behaviour for compression (a) parallel and (b) perpendicular to the build layers

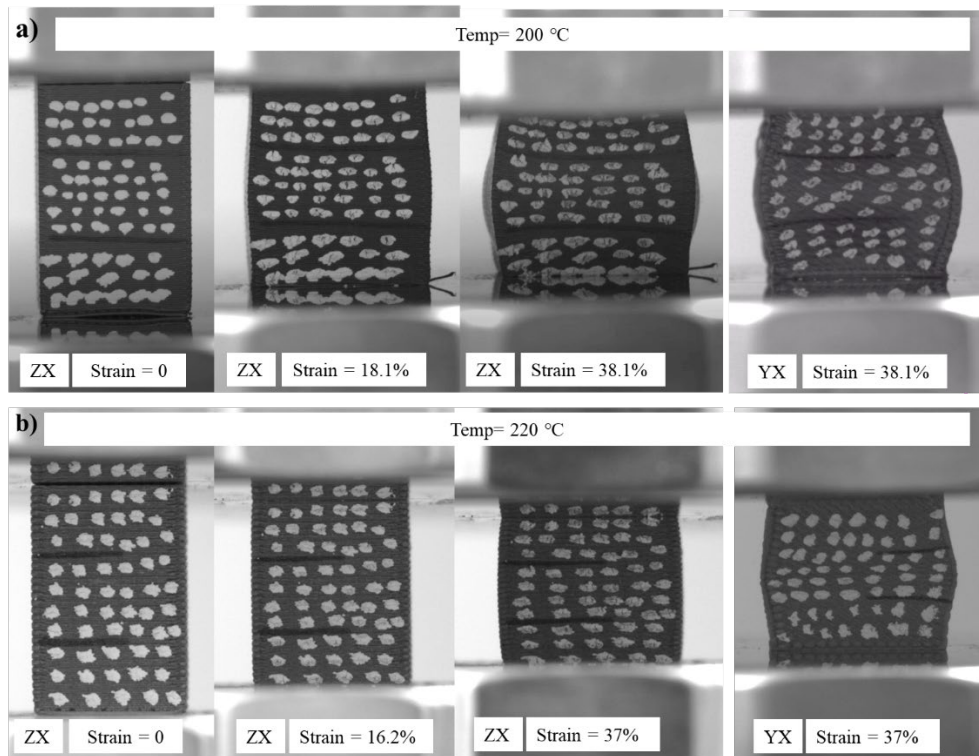


Figure 6: Compression testing of specimens printed with two different deposition temperatures (a) 200 °C (b) 220 °C

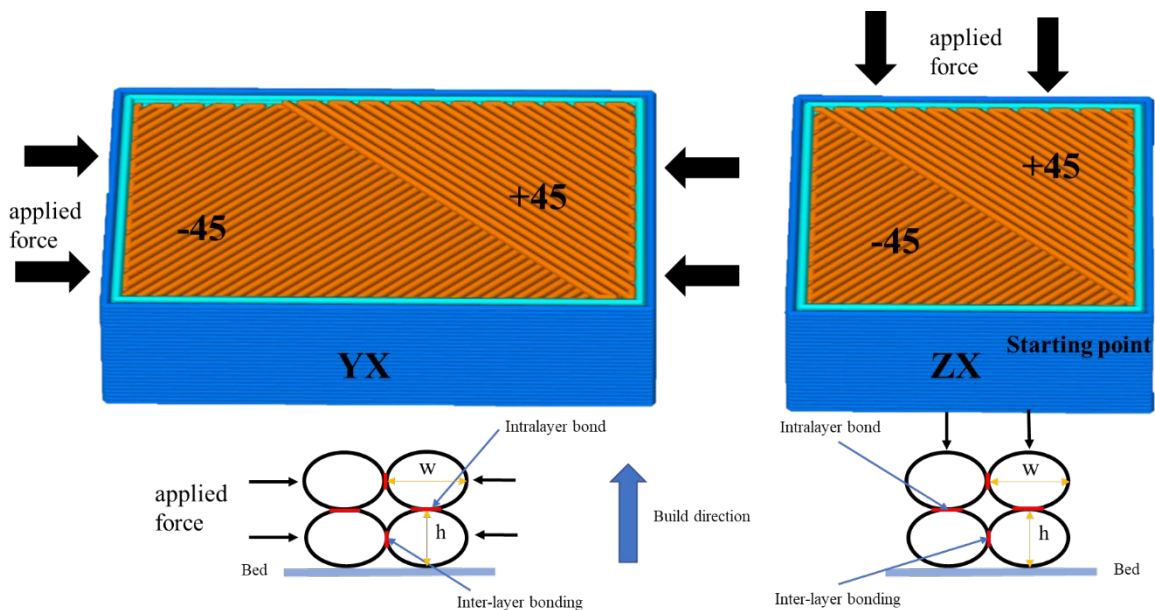


Figure 7: Schematics of the direction of infill and foaming expansion in relation to the applied force for compression force parallel and perpendicular to the build layers

Table 2 presents a summary of the mechanical properties **for foamed and non-foamed compression** samples, including the Young's modulus, energy absorbed and the energy absorption efficiency. The Young's Modulus for the non-foamed material (2966 MPa) is in keeping with values in the literature (typically between 2684 [25] and 3500 MPa [26]). Table 2 shows that, much like the yield stress, the Young's Modulus and energy absorbed (per unit mass or volume) decrease with decreasing density and that, with the exception of the non-foamed sample, all the measured properties are reduced when

compressing perpendicular to the layers (even though there are some small density differences for these samples).

Also presented in this table is the performance or merit index for a light stiff beam (based on the approach by Ashby [27] – where it is assumed here that the compressive Young's Modulus is a reliable indicator of the flexural modulus). The higher the index, the lighter the beam for the same nominal deflection under a given load. The foams all outperform the non-foamed beam, with up to 50% weight savings being possible. Since the Young's Modulus is lower for foams loaded perpendicular to the layers, so are the performance indices and mass savings. It is notable that, despite the different foaming behaviour in [19], the merit indices for the non-foamed and foamed PLA are very similar to those measured in this study.

Table 2: Summary of mechanical testing data for samples printed at different temperatures

Temp (°C)	Test to layer Direction	E (MPa)	σ_y (MPa)	$\sigma_{0.3}$ (MPa)	Density (g/cc)	E abs (MJ/m ³)	E abs (kJ/kg)	E eff (%)	E ^{1/3} / ρ
200		2966±56.5	60.0±1.25	50.9±0.22	1.24±0.05	13.8	11.2	77	11.6
	⊥	2960±62.5	61.3±0.915	54.6±0.66	1.23±0.035	14.8	12.0	80	11.6
210		1651±58.5	28.6±0.685	28.6±0.33	0.78±0.06	7.9	10.2	92	15.2
	⊥	1307±56.5	21.3±0.625	31.8±0.23	0.77±0.04	7.3	9.4	76	14.2
220		1028±22.71	19.0±0.65	16.5±0.12	0.59±0.04	4.6	7.8	81	17.1
	⊥	581±19.5	11.5±0.28	17.8±0.07	0.58±0.05	3.6	6.2	67	14.4
230		1185±34.4	19.7±0.615	17.6±0.1	0.64±0.04	5.0	7.8	84	16.5
	⊥	324±16.0	8.2±0.175	21.4±0.37	0.61±0.02	3.4	5.4	53	11.6
240		1366±41.5	19.6±0.615	18.5±0.55	0.74±0.05	5.1	6.9	87	15.0
	⊥	630±18.0	13.0±0.38	29.4±0.67	0.71±0.04	5.0	7.0	57	12.1

Figure 8 shows densities for foamed (220 °C, EM = 0.5) and non-foamed (200 °C, EM=0.9) samples and, for both cases, shows an approximately linear relationship between infill percentage and density. The density at 50% infill is greater than half that for the solid, because a two-track thick perimeter exists around the sample. At 20% infill, it is clear that a very open structure exists, albeit with a solid perimeter.

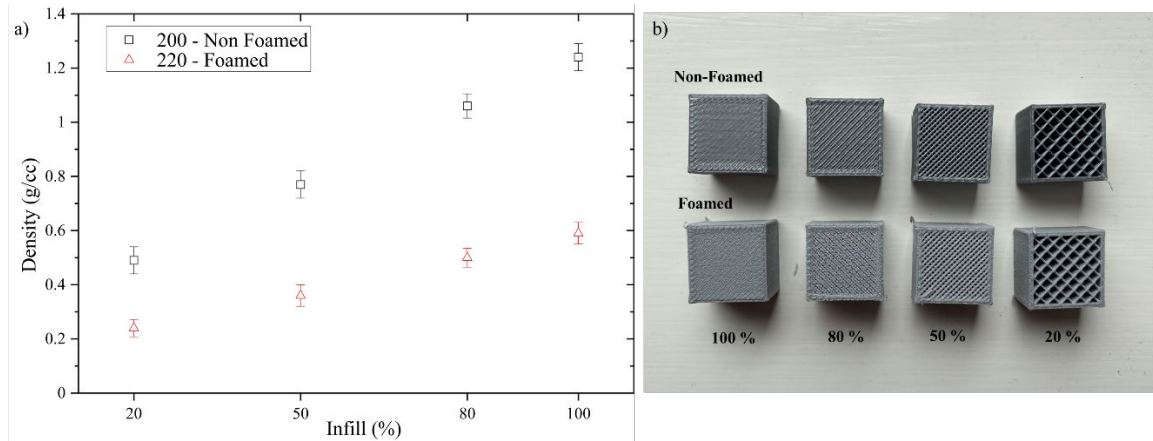


Figure 8: (a) The effect of infill percentage on the density of the foamed and non-foamed PLA and (b) the representative cubes with different infill in the ZX direction

Figure 10 shows the effect of infill percentage on the compressive stress-strain curves for foamed and non-foamed PLA parallel and perpendicular to the layers and Table 3 presents a summary of the mechanical properties for these samples. In general, the stress-strain curves are very similar in form to those presented for the solid blocks, with the exception of the highly pronounced drops in load for the very weak samples with 20% infill. It is clear from the figures that, as before, as the density decreases, so do the yield and plateau stresses. Changing the print direction from YX to ZX decreases the stiffness and yield strength for the foamed samples, as was observed earlier for samples with 100% infill. The effect is not the same for the non-foamed samples. The stiffness still decreases when changing the print direction from YX to ZX, but the compressive yield strength increases, although this is clouded somewhat by density increases for these samples. The same conclusion was reached for ABS material in [28].

In non-foamed PLA, the higher yield strength of the ZX samples can be justified by the location of the gap between the infill and outer wall in relation to the applied force. In YX samples, the gaps (A, B and C) shown in Figure 9 will behave as an energy absorber (much like the honeycomb in [29]) between the raster lines and will collapse progressively when the yield stress is reached. This results in low yield strength and a plateau type stress-strain curve. However, the gaps in the ZX samples leave a columnar structure, which is rigid and crushes after the yield point, resulting in densification.

The foamed samples tend to show a greater degree of anisotropy in performance. This can be associated with foaming expansion (gas bubbles) that creates irregular voids inside raster lines. The uneven surface of the tracks causes weaker bonding between raster lines, making the foam samples more sensitive to print direction. As a result, factors such as the direction of the raster lines in relation to the applied force, the quality of bonding between raster lines and the amount of material used in the structure play significant roles in the mechanical response.

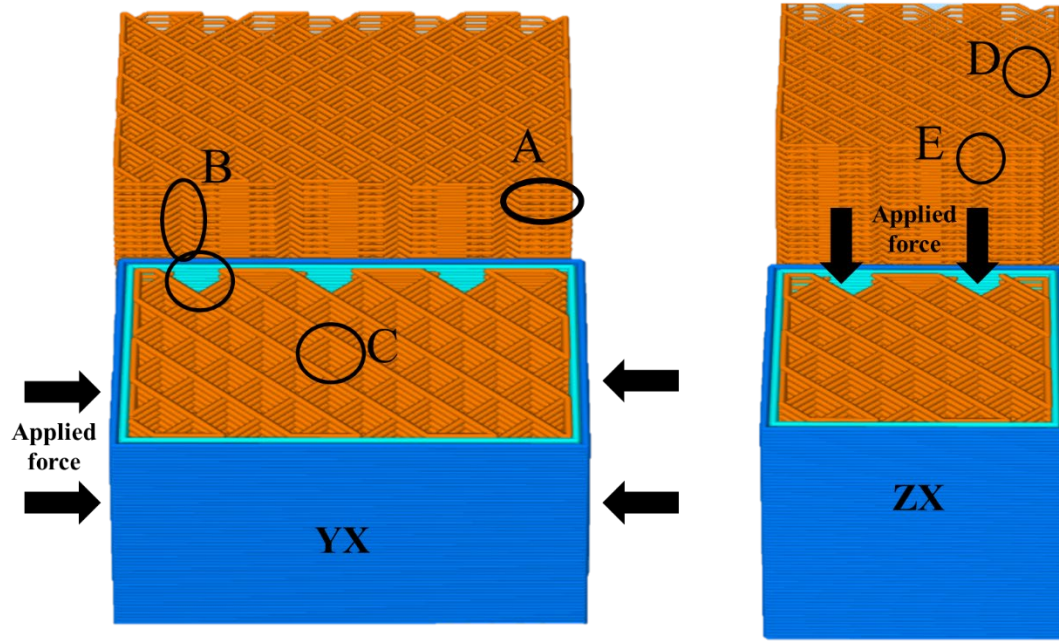


Figure 9: Schematics of the filling patterns and applied force direction in relation to the infill direction

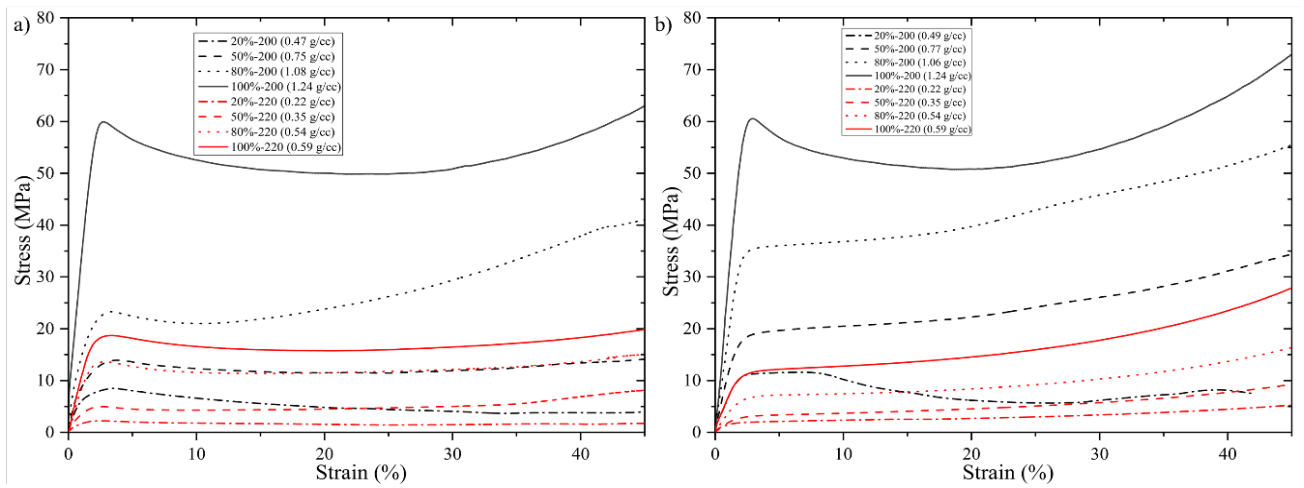


Figure 10: The effect of the infill percentage on the compressive stress-strain (a) parallel and (b) perpendicular to the layers

Table 3: Summary of mechanical testing data for samples printed at different temperatures, with different infill

Temp=200 (°C), EM=0.9									
Infill (%)	Test to layer Direction	E (MPa)	σ_y (MPa)	$\sigma_{0.3}$ (MPa)	Density (g/cc)	E abs (J/m ³)	E abs (J/kg)	E eff	E ^{1/3} / ρ
100		2966±56.5	60.0±1.25	50.9±0.22	1.24±0.05	13.8	11.2	77	11.6
	⊥	2960±62.5	61.3±0.915	54.6±0.66	1.23±0.035	14.8	12.0	80	11.7
80		2227±39	23.3±0.435	29.4±0.21	1.04±0.045	6.8	6.3	77	12.6
	⊥	2100±60	34.9±0.36	45.9±0.57	1.06±0.04	11.2	10.6	82	12.1
50		1119±70.5	13.9±0.49	11.9±0.52	0.75±0.05	3.5	4.7	85	13.8
	⊥	1063±14	17.7±0.73	26.1±0.54	0.77±0.025	6.3	8.1	80	13.3
20		724±22	8.5±0.3	4.1±0.01	0.48±0.05	1.7	3.5	67	18.7
	⊥	583±21	10.7±0.48	6.2±0.04	0.49±0.04	2.3	4.7	71	17.0
Temp=220 (°C), EM=0.5									
100		1028±22.7	19.0±0.65	16.5±0.12	0.59±0.04	4.6	7.8	81	17.1
	⊥	581±19.5	11.5±0.28	17.8±0.07	0.58±0.05	3.6	6.2	67	14.4
80		798±30	13.8±0.39	12.2±0.07	0.53±0.03	3.5	6.5	84	17.5
	⊥	419±21.5	6.5±0.29	10.3±0.13	0.50±0.03	2.3	4.7	76	15.0
50		400±16.78	4.9±0.1	5.0±0.16	0.35±0.04	1.32	3.77	90	21.1
	⊥	185±3	2.9±0.185	5.7±0.08	0.36±0.05	1.21	3.36	70	15.8
20		227±9	2.3±0.125	2.0±0.04	0.22±0.032	0.61	2.27	88	27.7
	⊥	153±9.5	1.8±0.05	3.4±0.08	0.24±0.04	0.74	3.08	73	22.3

The data in Table 3 can be analysed in terms of the performance and density relative to that **for non-foamed solid PLA** tested in the same direction. This analysis is convenient but is unable to separate contributions from the porosity within and between the tracks. Figure 11 shows examples of this analysis for the different properties. It is apparent that the changes in properties are a close fit to a power law, consistent with that commonly observed for porous materials. The foam data, shown as red squares in each plot, because of the included porosity within **the raster lines**, sit at lower relative densities, but there is some overlap with the **porous non-foamed structures**. The good fit to a single curve suggests, given the typical experimental scatter in data, that the fraction of porosity governs the behaviour, rather than the means by which it was introduced (**either into the raster or as gaps between the raster lines**).

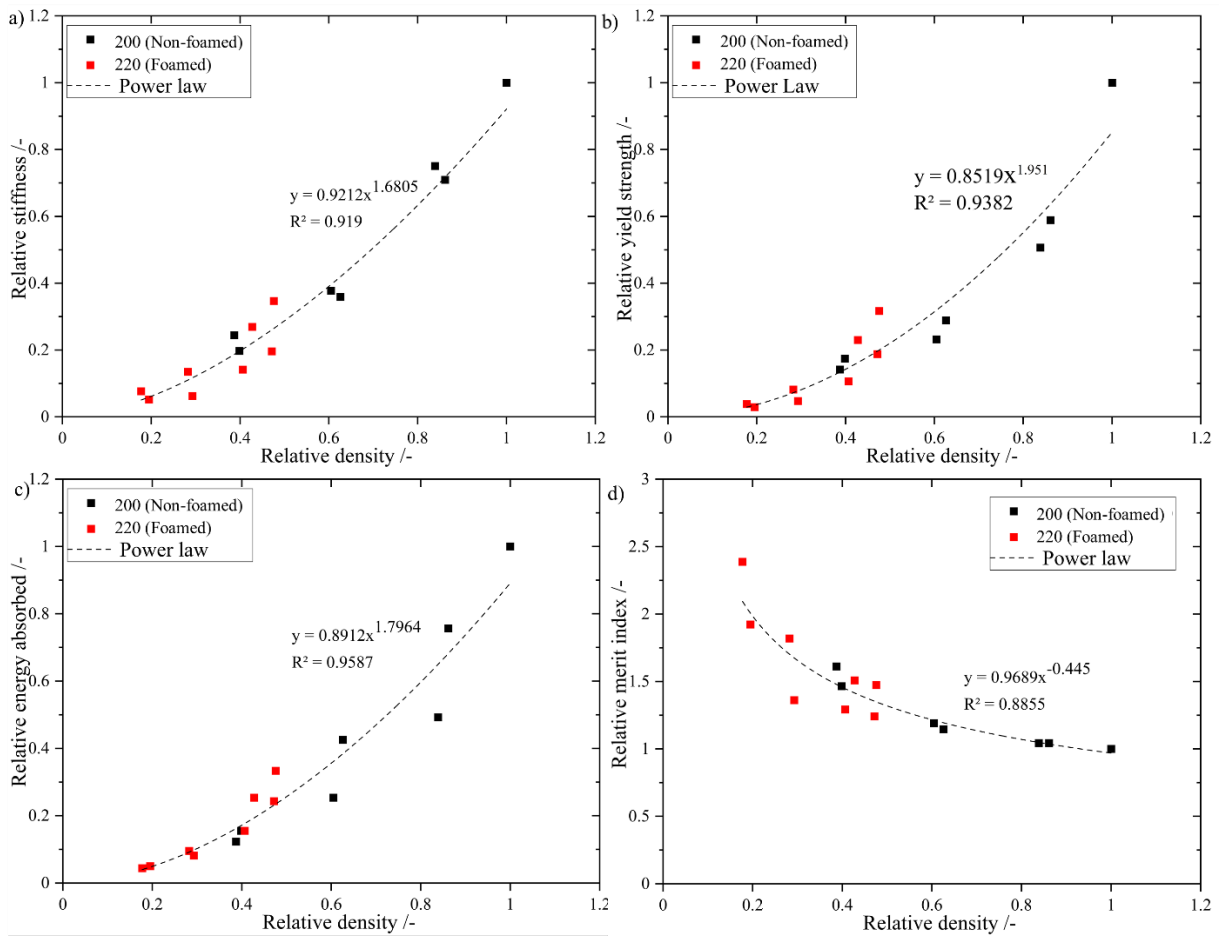


Figure 11: Plots of relative properties against relative density for a) stiffness, b) strength, c) energy absorbed per unit mass and d) merit index (equations and fits to all the data are shown in each figure)

To further the understanding, it is important to consider the change in properties as the infill fraction increases for both foamed and non-foamed track material. Figure 12 plots "normalised" relative mechanical properties and density. The relative properties have been normalised for both the foamed and non-foamed builds, to that for the corresponding material with 100% infill in the corresponding test direction, thereby only considering the effect of infill fraction on the properties. The data are clustered in four regions, corresponding to the four infill levels. The changes in properties are again a close fit to a power law with the foamed and non-foamed data fitting well, considering experimental scatter, to a single curve. This confirms the same change in properties with infill fraction, irrespective of the structure or properties of the track material (foamed or non-foamed).

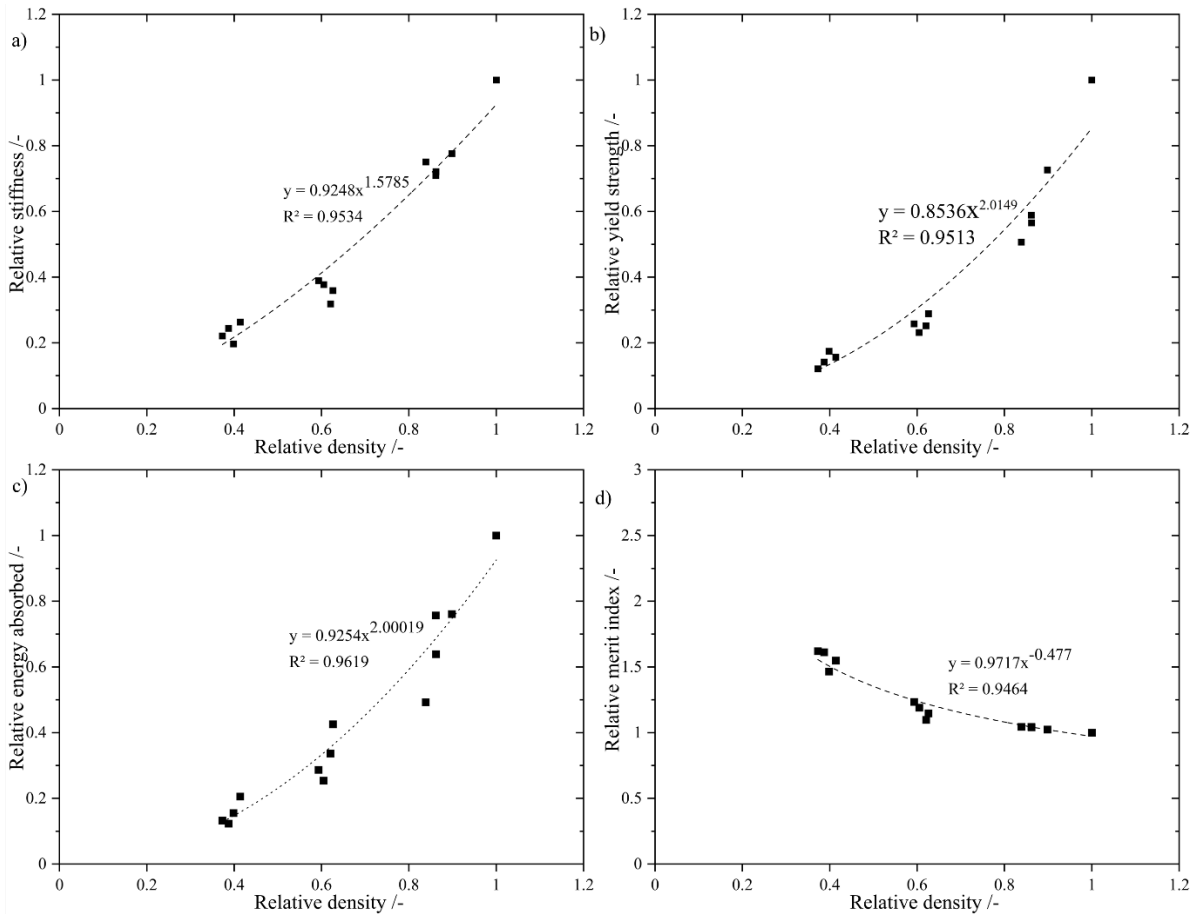


Figure 12: Plots of normalised relative properties against normalised relative density for a) stiffness, b) strength, c) energy absorbed per unit mass and d) merit index (equations and fits to all the data are shown in each figure)

Whilst there is no apparent benefit in the mechanical performance of introducing porosity into a polymer via either foaming or partial infilling, the foamable filament does offer some advantages over a simple infill approach. In combination with infill, it offers a route to low solid fractions and low densities and with that, high merit indices that make these structures highly suitable for lightweight beams. Porous structures for energy absorption with high efficiencies are also possible, and foaming offers a route to this (and stiff - lightweight structures) if components with low fractions of interconnected porosity are required. A disadvantage of the structures produced thus far is the more pronounced anisotropic behaviour of the foamed components, even for those with 100% infill.

A possible approach to mitigating this is to combine the previous approaches. In this way, the filament is heated sufficiently to induce foaming (i.e. to 220°C) but the EM is not reduced (it remains 0.9). To accommodate the excess extrusion of material from the nozzle, printing with partial infill is used, allowing the excess material to flow into the free space between tracks. Under the conditions mentioned above, the foaming process approximately doubles the volume, meaning a sensible infill to use is 50%. Figure 13 confirms this premise and shows that, for an infill of 80%, the vacant volume was insufficient for foam expansion and led to over-building, while for an infill of 20%, there was still free space. As expected, for an infill of 50%, a build was produced within the acceptable tolerance range. Figure 14

shows how the foam printed with EM=0.9 has flowed into neighbouring vacant spaces for a 50% infill, leading to nearly double the track width (but the same track height).

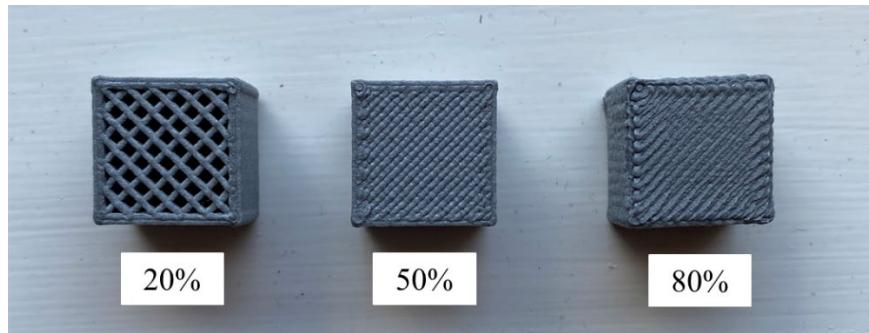


Figure 13: Printed foam PLA at 220C with EM of 0.9 and various infill

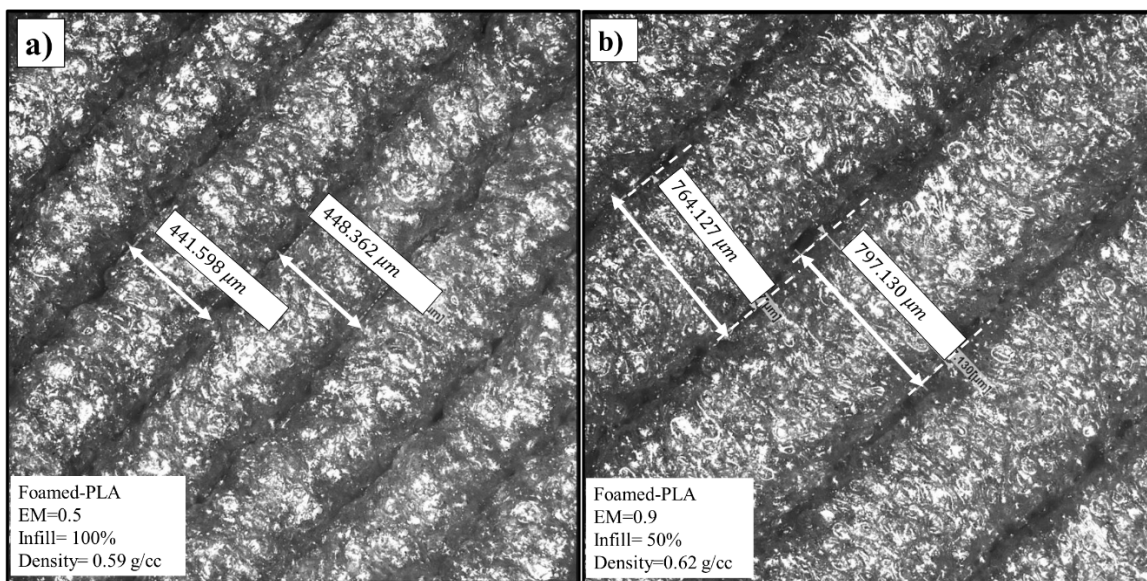


Figure 14: The comparison of the raster lines for foamed-PLA with two different processing parameters (a) EM=0.5 and density= 0.59 g/cc (b) EM=0.9 and density= 0.62 g/cc

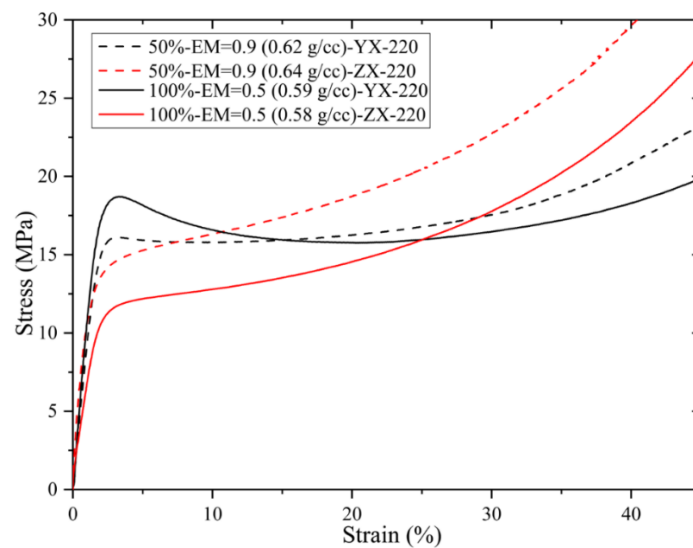


Figure 15: compressive stress-strain for foamed structures printed with EM=0.9 and EM=0.5 for two different build directions

Table 4: Comparison of mechanical testing data for foamed samples printed with different EM and infill

Infill (%)	Test to layer Direction	E (MPa)	σ_y (MPa)	$\sigma_{0.3}$ (MPa)	Density (g/cc)	E abs (J/m ³)	E abs (J/kg)	E eff	$E^{1/3}/\rho$
Temp=220 (°C), EM=0.5									
100		1028±22.71	19.0±0.65	16.5±0.12	0.59±0.04	4.6	7.8	81	17.1
	⊥	581±19.5	11.5±0.28	17.8±0.07	0.58±0.05	3.6	6.2	67	14.4
Temp=220 (°C), EM=0.9									
50		901±28.5	16.1±0.145	17.6±0.124	0.61±0.02	4.7	7.7	89	15.8
	⊥	1038±102	13.6±0.55	22.0±0.845	0.63±0.04	5.2	8.2	76	16.1

Table 4 shows that the density of the printed cube with 100% infill and EM=0.5 is fairly close to the density of the cube with 50% infill and EM=0.9. To optimise this, the infill would need to be a little lower. Although the slight difference in density makes direct comparison a little difficult, it is apparent that the properties are less anisotropic, most notably the Young's modulus.

As previously mentioned, the highest strength in foam samples was obtained when the rasters and loads were oriented in the same direction (YX direction). The new printing approach improved properties in the ZX but not the YX direction samples. Specimens with lower infill and higher EM values have fewer, thicker raster lines (as was evident in Figure 14). This is similar to using a larger nozzle size, which allows more molten material to be deposited and can decrease porosity in the necked area between raster lines [30]. Thermal history of the raster lines also plays a crucial role in the quality of the bonding. The ZX samples, with shorter times between successive layers, benefit, in terms of interlayer bonding strength, from higher heat retention between raster lines and layers [31].

Printing with partial infill and high EM is likely to be more attractive for creating complex solid parts with foamable filament that require an isotropic mechanical response as using a lower infill percentage and a higher flow rate will require significantly lower printing times. The benefits of a larger track size in terms of speed come from the ability to do fewer perimeters for a given wall thickness and fewer raster lines in the inner infill.

Conclusions

Foamed PLA specimens were fabricated using MEX 3D printers with a maximum foaming expansion being achieved at an extrusion nozzle temperature of 220°C. To achieve dimensional accuracy, the extrusion multiplier value had to be decreased to compensate for foam expansion. As the maximum foam expansion observed was close to 100%, the extrusion multiplier was reduced to 0.5. Similar accurate builds using foamable filament could be achieved using an extrusion multiplier of 0.9 but by decreasing the infill to 50%. The resulting thicker raster lines led to shorter build times.

The compressive properties of foamed cubes decreased with increasing porosity (decreasing density) and showed anisotropic behaviour, with strength and stiffness being lower when samples were compressed perpendicular to the build layers. This behaviour was attributed to the greater sensitivity of the loading direction relative to foamed raster lines with rough surfaces.

The mechanical performance of these foamed materials follows power-law functions of the relative density (or solid fraction). Analysis of these trends indicated that the mechanical response was, within experimental scatter, a function of the overall solid fraction and not the type of porosity (in the raster or between the raster lines). Analysis based on the effect of infill alone showed the same changes in properties irrespective of the porosity level contained in the raster lines.

Although introducing porosity into a polymer via foaming or partial infilling has no apparent benefit to the mechanical performance, foamable filaments can offer some advantages over a simple infill approach if stiff, lightweight structures with low fractions of interconnected porosity are required. In combination with infill, it offers a practical route to low solid fractions and structures with high merit indices that would be highly suitable cores in novel sandwich structures for lightweight beams.

CRedit authorship contribution statement

Armin Yousefi Kanani: Conceptualisation, Methodology, Experimental test, Writing - original draft.

Andrew Kennedy: Conceptualisation, Methodology, writing- review and editing.

Acknowledgement:

This work is financially supported by the European Regional Development Fund through the Greater Innovation for Smart Materials Optimisation (GISMO) Project (grant reference number 03R18P02671).

Declaration of Competing Interest

The authors declare that they have no known competing financial interests or personal relationships that could have influenced the work reported in this paper.

Reference

- [1] G. Coste, C. Negrell and S. Caillol, "From gas release to foam synthesis, the second breath of blowing agents," *Eur. Polym. J.*, vol. 140, no. September, p. 110029, Nov. 2020, doi: 10.1016/j.eurpolymj.2020.110029.
- [2] E. Di Maio and E. Kiran, "Foaming of polymers with supercritical fluids and perspectives on the current knowledge gaps and challenges," *J. Supercrit. Fluids*, vol. 134, pp. 157–166, Apr. 2018, doi: 10.1016/j.supflu.2017.11.013.
- [3] F.-L. Jin, M. Zhao, M. Park and S.-J. Park, "Recent Trends of Foaming in Polymer Processing: A Review," *Polymers (Basel)*, vol. 11, no. 6, p. 953, Jun. 2019, doi: 10.3390/polym11060953.
- [4] N. Gama, A. Ferreira and A. Barros-Timmons, "Polyurethane Foams: Past, Present, and Future," *Materials (Basel)*, vol. 11, no. 10, p. 1841, Sep. 2018, doi: 10.3390/ma11101841.
- [5] I. Tsivintzelis, A. G. Angelopoulou and C. Panayiotou, "Foaming of polymers with

- supercritical CO₂: An experimental and theoretical study," *Polymer (Guildf.)*, vol. 48, no. 20, pp. 5928–5939, Sep. 2007, doi: 10.1016/j.polymer.2007.08.004.
- [6] M. A. Rodríguez-Pérez, "Crosslinked Polyolefin Foams: Production, Structure, Properties, and Applications," in *Advances in Polymer Science*, vol. 184, no. July, 2005, pp. 97–126. doi: 10.1007/b136244.
- [7] G. Wypych, *Handbook of Foaming and Blowing Agents*. ChemTec Publishing. ChemTec Publishing, 2017. [Online]. Available: <https://app.knovel.com/hotlink/toc/id:kpHFBA0009/handbook-foaming-blowing/handbook-foaming-blowing>
- [8] J. Stehr, "Chemical Blowing Agents in the Rubber Industry. Past – Present – and Future?," *Int. Polym. Sci. Technol.*, vol. 43, no. 5, pp. 1–10, May 2016, doi: 10.1177/0307174X1604300501.
- [9] B. R. Bharath Kumar, M. Doddamani, S. E. Zeltmann, N. Gupta, M. R. Ramesh and S. Ramakrishna, "Processing of cenosphere/HDPE syntactic foams using an industrial scale polymer injection molding machine," *Mater. Des.*, vol. 92, pp. 414–423, Feb. 2016, doi: 10.1016/j.matdes.2015.12.052.
- [10] A. K. Singh, B. Patil, N. Hoffmann, B. Saltonstall, M. Doddamani and N. Gupta, "Additive Manufacturing of Syntactic Foams: Part 1: Development, Properties, and Recycling Potential of Filaments," *JOM*, vol. 70, no. 3, pp. 303–309, Mar. 2018, doi: 10.1007/s11837-017-2734-7.
- [11] M. Sauceau, J. Fages, A. Common, C. Nikitine and E. Rodier, "New challenges in polymer foaming: A review of extrusion processes assisted by supercritical carbon dioxide," *Prog. Polym. Sci.*, vol. 36, no. 6, pp. 749–766, Jun. 2011, doi: 10.1016/j.progpolymsci.2010.12.004.
- [12] C. Zhou, P. Wang and W. Li, "Fabrication of functionally graded porous polymer via supercritical CO₂ foaming," *Compos. Part B Eng.*, vol. 42, no. 2, pp. 318–325, 2011, doi: 10.1016/j.compositesb.2010.11.001.
- [13] P. Song, C. Zhou, H. Fan, B. Zhang, X. Pei, Y. Fan, Q. Jiang, R. Bao, Q. Yang, Z. Dong, *et al.*, "Novel 3D porous biocomposite scaffolds fabricated by fused deposition modeling and gas foaming combined technology," *Compos. Part B Eng.*, vol. 152, no. April, pp. 151–159, 2018, doi: 10.1016/j.compositesb.2018.06.029.
- [14] W. J. Choi, K. S. Hwang, H. J. Kwon, C. Lee, C. H. Kim, T. H. Kim, S. W. Heo, J.-H. Kim and J.-Y. Lee, "Rapid development of dual porous poly(lactic acid) foam using fused deposition modeling (FDM) 3D printing for medical scaffold application," *Mater. Sci. Eng. C*, vol. 110, no. September 2019, p. 110693, May 2020, doi: 10.1016/j.msec.2020.110693.
- [15] A. R. Damanpack, A. Sousa and M. Bodaghi, "Porous PLAs with Controllable Density by FDM 3D Printing and Chemical Foaming Agent," *Micromachines*, vol. 12, no. 8, p. 866, Jul. 2021, doi: 10.3390/mi12080866.
- [16] RichRap3D, "ColorFabb LW-PLA Expanding Foaming Plastic Filament for 3D Printing - Part 1 Testing and experimentation," 2019. <https://richrap.blogspot.com/2019/04/colorfabb-lw-pla-expanding-foaming.html> (accessed Oct. 03, 2021).
- [17] S. Hermann, "COLORFABB LW-PLA TESTING FOAMING PLA," 2020. <https://www.cnckitchen.com/blog/colorfabb-lw-pla-testing-foaming-pla> (accessed Oct. 03, 2021).
- [18] Y. Tao, F. Kong, Z. Li, J. Zhang, X. Zhao, Q. Yin, D. Xing and P. Li, "A review on voids of 3D printed parts by fused filament fabrication," *J. Mater. Res. Technol.*, vol. 15, pp. 4860–4879, Nov. 2021, doi: 10.1016/j.jmrt.2021.10.108.
- [19] H. E. Naguib, C. B. Park and N. Reichelt, "Fundamental foaming mechanisms governing the volume expansion of extruded polypropylene foams," *J. Appl. Polym. Sci.*, vol. 91, no. 4, pp.

- 2661–2668, Feb. 2004, doi: 10.1002/app.13448.
- [20] A. El Magri, K. El Mabrouk, S. Vaudreuil and M. E. Touhami, "Mechanical properties of CF-reinforced PLA parts manufactured by fused deposition modeling," *J. Thermoplast. Compos. Mater.*, vol. 34, no. 5, pp. 581–595, 2021, doi: 10.1177/0892705719847244.
- [21] S. Guessasma, S. Belhabib and H. Nouri, "Thermal cycling, microstructure and tensile performance of PLA-PHA polymer printed using fused deposition modelling technique," *Rapid Prototyp. J.*, vol. 26, no. 1, pp. 122–133, Jan. 2020, doi: 10.1108/RPJ-06-2019-0151.
- [22] H. S. Kim and P. Plubrai, "Manufacturing and failure mechanisms of syntactic foam under compression☆," *Compos. Part A Appl. Sci. Manuf.*, vol. 35, no. 9, pp. 1009–1015, Sep. 2004, doi: 10.1016/j.compositesa.2004.03.013.
- [23] J. Zhang, N. Kikuchi, V. Li, A. Yee and G. Nusholtz, "Constitutive modeling of polymeric foam material subjected to dynamic crash loading," *Int. J. Impact Eng.*, vol. 21, no. 5, pp. 369–386, 1998, doi: 10.1016/s0734-743x(97)00087-0.
- [24] A. C. Abbott, G. P. Tandon, R. L. Bradford, H. Koerner and J. W. Baur, "Process-structure-property effects on ABS bond strength in fused filament fabrication," *Addit. Manuf.*, vol. 19, pp. 29–38, Jan. 2018, doi: 10.1016/j.addma.2017.11.002.
- [25] M. Mansour, K. Tsongas and D. Tzetzis, "Measurement of the mechanical and dynamic properties of 3D printed polylactic acid reinforced with graphene," *Polym. Technol. Mater.*, vol. 58, no. 11, pp. 1234–1244, Jul. 2019, doi: 10.1080/03602559.2018.1542730.
- [26] P. Vatsh and K. Sahu, "Comparison of Most Suitable 3D Printing Materials , Failure Testing of PLA and ABS and Experimental Testing of PLA by Instron Machine," vol. 5, no. 07, pp. 760–765, 2017.
- [27] M. F. Ashby, *Materials Selection in Mechanical Design*. Elsevier, 2011. doi: 10.1016/C2009-0-25539-5.
- [28] K. Upadhyay, R. Dwivedi and A. K. Singh, "Determination and Comparison of the Anisotropic Strengths of Fused Deposition Modeling P400 ABS," in *Advances in 3D Printing & Additive Manufacturing Technologies*, Singapore: Springer Singapore, 2017, pp. 9–28. doi: 10.1007/978-981-10-0812-2_2.
- [29] L. Yan, K. Zhu, Y. Zhang, C. Zhang and X. Zheng, "Effect of Absorbent Foam Filling on Mechanical Behaviors of 3D-Printed Honeycombs," *Polymers (Basel)*, vol. 12, no. 9, p. 2059, Sep. 2020, doi: 10.3390/polym12092059.
- [30] J. Triyono, H. Sukanto, R. M. Saputra and D. F. Smaradhana, "The effect of nozzle hole diameter of 3D printing on porosity and tensile strength parts using polylactic acid material," *Open Eng.*, vol. 10, no. 1, pp. 762–768, Aug. 2020, doi: 10.1515/eng-2020-0083.
- [31] B. Akhouni and A. H. Behraves, "Effect of Filling Pattern on the Tensile and Flexural Mechanical Properties of FDM 3D Printed Products," *Exp. Mech.*, vol. 59, no. 6, pp. 883–897, Jul. 2019, doi: 10.1007/s11340-018-00467-y.

